In-plane formation reconfiguration with radial maneuvers

Lim, Yeerang; Mok, Sung Hoon

DOI
10.2514/1.G004933

Publication date
2020

Document Version
Final published version

Published in
Journal of Guidance, Control, and Dynamics

JOURNAL OF GUIDANCE, CONTROL, AND DYNAMICS
Vol. 43, No. 10, October 2020

In-Plane Formation Reconfiguration with Radial Maneuvers

Yeerang Lim*
Technical University of Berlin, 10623 Berlin, Germany
and
Sung-Hoon Mok†
Delft University of Technology, 2629 HS Delft, The Netherlands

https://doi.org/10.2514/1.G004933

Formation reconfiguration with impulsive maneuvers has been continuously addressed in recent decades. The studies mostly focused on in-plane formation reconfiguration since the out-of-plane motion is independently controlled by a single burn. Most in-plane reconfiguration studies, meanwhile, rely on tangential maneuvers because of fuel efficiency and controllability of the orbital energy, compared to radial maneuvers. In this paper, the perspective differs that little influence of the radial maneuvers on the orbital energy is considered as a benefit rather than a drawback. By employing radial burns only, an effect of the thrust errors on the semimajor axis control error can be minimized. Both numerical simulations and sensitivity analysis demonstrate the robustness of the proposed radial impulsive burns compared to the conventional tangential impulsive control schemes.

Nomenclature

a	=	semimajor axis
e	=	eccentricity
i	=	inclination
M	=	mean anomaly
n	=	mean orbit velocity
R_E	=	Earth radius
u	=	mean argument of latitude
$\Delta V_R, \Delta V_T, \Delta V_N$	=	velocity changes in local radial, tangential, and normal directions
$\delta \boldsymbol{e}$	=	$[\delta e_x \quad \delta e_y]^T$; relative eccentricity vector
$\delta \boldsymbol{i}$	=	$[\delta i_x \quad \delta i_y]^T$; relative inclination vector
$\delta\lambda$	=	relative longitude
θ	=	argument of latitude of the relative ascending node
φ	=	argument of latitude of the relative perigee
Ω	=	right ascension of the ascending node
ω	=	argument of perigee

I. Introduction

IMPULSIVE control for formation reconfiguration has been continuously studied in the past decades because it is the key to substantializing a space mission with multiple satellites. The methods can be roughly divided into two parts: one with relative Cartesian coordinates [1–3] and the other with orbit elements difference [4–12]. Concentrating on the latter part, Schaub and Alfriend [6] proposed an analytical solution consisting of three impulses. An impulse pair whose firing locations are separated by a half-orbit period was applied for in-plane correction. Both tangential and radial delta-v components were employed at the two extreme points: perigee and apogee. Vaddi et al. [7] derived an analytical two-impulse maneuver strategy for projected circular orbit reconfiguration. The first delta-v vector was composed of radial and orbit-normal components, and the second delta-v vector was only in the radial direction. To reduce delta-v consumption further, multiple-revolution solutions have also been sought [12–15], assuming a control window of longer than an orbital period. Mok et al. [12] expanded upon the previous solution [6] by adding a pair of tangential impulses to exploit along-track drift in reducing the total delta-v cost.

Aiming at real implementations of formation control, D'Amico and Montenbruck [8] developed an analytical fuel-efficient control strategy for the TanDEM-X mission, based on relative orbit elements' (ROE') representation [9]. For in-plane correction, two tangential impulses were applied, which are in terms of four ROE components: relative semimajor axis (SMA), two-element relative eccentricity vector, and relative longitude. However, the relative longitude could not be tightly controlled due to the limited number of impulses. In 2015, Gaias and D'Amico [10] generalized the previous study by considering the use of radial and tangential impulses together. Especially, the proposed three-tangential-impulsive strategy was able to further reduce delta-v consumption and tightly control the relative longitude. In 2018, the three-impulse strategy was applied as one of the orbit control solutions for optimal maneuver planning of reconfiguration [11].

While there is a significant benefit of employing only tangential impulses in formation control regarding fuel efficiency, two side effects might be present. One is a longer reconfiguration period compared to the general impulsive strategy (employing both tangential and radial maneuvers) which requires less than 1.5 orbital periods to accomplish the reconfiguration [6,7]. This is due to the intermediate time used to exploit the drift motion caused by the SMA difference in order to reduce the delta-v cost. The second is an impact of the thrust execution error on the ROE control. When the desired along-track drift motion is not exactly induced or is not fully eliminated after reconfiguration by the thrust error, it can cause an extra drift motion. This can be problematic for safety if the relative eccentricity/inclination (e/i) vectors are not maintained in parallel. For example, in formation flying with smaller spacecraft (e.g., CubeSats), periodic formation keeping against the J2 perturbation may not be feasible due to the limited amount of fuel [16]. In this case, the safety condition is dependent on the relative longitude (i.e., along-track offset), therefore the relative longitude drift caused by the thrust error can raise the safety issue.

In this paper, the reconfiguration problem is formulated by employing only radial impulses. Analytical delta-v solutions for two and three impulses are newly obtained. A required reconfiguration time is less than 1.5 orbital periods which is aligned with previous studies [6,7]. Another important benefit of the proposed method is that the relative SMA is hardly changed after the reconfiguration maneuver since it is only affected by the tangential delta-v component. Hence, the unintended along-track drift motion that might threaten the safety requirement can be avoided. The controllability of

Received 2 November 2019; revision received 31 March 2020; accepted for publication 6 June 2020; published online 10 August 2020.

*Research Assistant, Chair of Space Technology, Faculty V; yeerang.lim@tu-berlin.de.

†Postdoctoral Researcher, Faculty of Aerospace Engineering; s.mok@tudelft.nl.

the SMA is assumed to be achieved by another orbit control method that is differential drag control [17–19], which has been already applied in several missions such as the constellation of Planet Labs Inc.' [17,18] and NASA's Cyclone Global Navigation Satellite System (CYGNSS) [19] constellations.

In the following part of the paper, Sec. II introduces the relative motion equations parameterized by ROE. Sections III and IV propose two- and three-radial-impulsive methods, respectively. Section V demonstrates the performance of the proposed method: especially focusing on its robustness against the thrust execution error. Finally, Sec. VI presents a systematic sensitivity study of both radial and tangential impulsive methods against the thrust error.

II. Relative Motion Equations

Relative motion between two spacecraft can be described by the relative orbit elements [9]:

$$\begin{pmatrix} \delta a \\ \delta e_x \\ \delta e_y \\ \delta i_x \\ \delta i_x \\ \delta\lambda \end{pmatrix} = \begin{pmatrix} \delta a \\ \delta e\cos\varphi \\ \delta e\sin\varphi \\ \delta i\cos\theta \\ \delta i\sin\theta \\ \delta\lambda \end{pmatrix} = \begin{pmatrix} (a_d - a)/a \\ e_d\cos\omega_d - e\cos\omega \\ e_d\sin\omega_d - e\sin\omega \\ i_d - i \\ (\Omega_d - \Omega)\sin i \\ (u_d - u) + (\Omega_d - \Omega)\cos i \end{pmatrix} \tag{1}$$

where $(a, e, \omega, i, \Omega, u)$ are the classical orbit elements (OE) of the chief satellite, except $u = M + \omega$ of the mean argument of latitude. The subscript d stands for the OE of the deputy satellite, $[\delta e_x \quad \delta e_y]^T$ is the relative eccentricity vector, and $[\delta i_x \quad \delta i_y]^T$ is the relative inclination vector. Compared to the Cartesian coordinate representation, the first five ROE components are kept constant in the Keplerian orbit. Even with major perturbations such as the J2 perturbation and aerodynamic drag, the ROE components are slowly varying so that the closed-form solution of the state transition matrix can be achieved [20].

Instantaneous change of the ROE by the impulsive maneuver can be represented by

$$a\begin{pmatrix} \Delta\delta a \\ \Delta\delta e_x \\ \Delta\delta e_y \\ \Delta\delta i_x \\ \Delta\delta i_x \\ \Delta\delta\lambda \end{pmatrix} = \frac{1}{n}\begin{bmatrix} 0 & 2 & 0 \\ \sin u & 2\cos u & 0 \\ -\cos u & 2\sin u & 0 \\ 0 & 0 & \cos u \\ 0 & 0 & \sin u \\ -2 & 0 & 0 \end{bmatrix}\begin{pmatrix} \Delta V_R \\ \Delta V_T \\ \Delta V_N \end{pmatrix} \tag{2}$$

In this equation, important relationships between the relative motion and delta-v maneuver can be found. First, the in-plane motion and the out-of-plane motion can be decoupled. Second, the tangential maneuver ΔV_T can control an eccentricity vector with half of delta-v expenditure compared to the radial maneuver ΔV_R. Third, the relative SMA $a\delta a$ can be only changed by the tangential maneuver. In this paper, assuming that $\Delta\delta a$ is zero, the two or three radial impulses are applied to correct $(\Delta\delta e_x, \Delta\delta e_y, \Delta\delta\lambda)$. In addition, the single orbit-normal impulse is applied to correct $(\Delta\delta i_x, \Delta\delta i_y)$ [10].

III. In-Plane Reconfiguration with Two Radial Maneuvers

The change of the ROE in the in-plane motion by radial impulse ΔV_R can be summarized as follows:

$$\begin{aligned} a\Delta\delta\lambda &= -2\Delta V_R/n \\ a\Delta\delta e_x &= \Delta V_R\sin u/n \\ a\Delta\delta e_y &= -\Delta V_R\cos u/n \end{aligned} \tag{3}$$

Supposing that the two radial impulses ΔV_{R_1} and ΔV_{R_2} are employed for reconfiguration, Eq. (3) can be rewritten by

$$\begin{aligned} a\Delta\delta\lambda &= -2\Delta V_{R_1}/n - 2\Delta V_{R_2}/n \\ a\Delta\delta e_x &= \Delta V_{R_1}\sin u_1/n + \Delta V_{R_2}\sin u_2/n \\ &= \Delta V_{R_1}\sin u/n + \Delta V_{R_2}\sin(u+\xi)/n \\ a\Delta\delta e_y &= -\Delta V_{R_1}\cos u_1/n - \Delta V_{R_2}\cos u_2/n \\ &= -\Delta V_{R_1}\cos u/n - \Delta V_{R_2}\cos(u+\xi)/n \end{aligned} \tag{4}$$

There are three equations with four unknown variables: ΔV_{R_1}, ΔV_{R_2}, u_1, and ξ, where u_1 represents the angular position at the first impulse firing; and $\xi = u_2 - u_1$ is the angular distance between the two impulses.

To obtain the minimum delta-v solution, a cost function J can be defined as a function of ΔV_{R_2}:

$$\begin{aligned} J \equiv |\Delta V_{R_1}| + |\Delta V_{R_2}| &= \left| -\frac{na\Delta\delta\lambda}{2} - \Delta V_{R_2} \right| + |\Delta V_{R_2}| \\ &= \left| \frac{na\Delta\delta\lambda}{2} + \Delta V_{R_2} \right| + |\Delta V_{R_2}| \end{aligned} \tag{5}$$

Assuming $\Delta\delta\lambda \geq 0$ without loss of generosity, J can be categorized into the three following cases:

Case a: $\Delta V_{R_2} < -\frac{na\Delta\delta\lambda}{2}$,

$$\begin{aligned} J &= \left| \frac{na\Delta\delta\lambda}{2} + \Delta V_{R_2} \right| + |\Delta V_{R_2}| = -\frac{na\Delta\delta\lambda}{2} - \Delta V_{R_2} - \Delta V_{R_2} \\ &= -\frac{na\Delta\delta\lambda}{2} - 2\Delta V_{R_2} \end{aligned} \tag{6}$$

Case b: $-\frac{na\Delta\delta\lambda}{2} \leq \Delta V_{R_2} \leq 0$,

$$\begin{aligned} J &= \left| \frac{na\Delta\delta\lambda}{2} + \Delta V_{R_2} \right| + |\Delta V_{R_2}| = \frac{na\Delta\delta\lambda}{2} + \Delta V_{R_2} - \Delta V_{R_2} \\ &= \frac{na\Delta\delta\lambda}{2} \end{aligned} \tag{7}$$

Case c: $\Delta V_{R_2} > 0$,

$$\begin{aligned} J &= \left| \frac{na\Delta\delta\lambda}{2} + \Delta V_{R_2} \right| + |\Delta V_{R_2}| = \frac{na\Delta\delta\lambda}{2} + \Delta V_{R_2} + \Delta V_{R_2} \\ &= \frac{na\Delta\delta\lambda}{2} + 2\Delta V_{R_2} \end{aligned} \tag{8}$$

Meanwhile, ΔV_{R_2} can be represented as a function of ξ. First, the last two equations of Eq. (4) can be organized as

$$a\Delta\delta e_x\sin u - a\Delta\delta e_y\cos u = \frac{1}{n}\Delta V_{R_1} + \frac{1}{n}\Delta V_{R_2}\cos\xi \tag{9}$$

$$a\Delta\delta e_x\cos u + a\Delta\delta e_y\sin u = \frac{1}{n}\Delta V_{R_2}\sin\xi \tag{10}$$

By combining Eqs. (9) and (10),

$$n^2a^2(\Delta\delta e_x^2 + \Delta\delta e_y^2) = \Delta V_{R_1}^2 + \Delta V_{R_2}^2 + 2\Delta V_{R_1}\Delta V_{R_2}\cos\xi \tag{11}$$

can be achieved. Substituting $2\Delta V_{R_1} = -na\Delta\delta\lambda - 2\Delta V_{R_2}$ from Eq. (4) into Eq. (11), the equation can be rewritten as follows:

$$\begin{aligned} n^2a^2(\Delta\delta e_x^2 + \Delta\delta e_y^2) = {} & n^2a^2\Delta\delta\lambda^2/4 + na\Delta\delta\lambda\Delta V_{R_2} + 2\Delta V_{R_2}^2 \\ & - na\Delta\delta\lambda\Delta V_{R_2}\cos\xi - 2\Delta V_{R_2}^2\cos\xi \end{aligned} \tag{12}$$

By rearranging Eq. (12) as an order of ΔV_{R_2}, the second-order equations can be achieved such that

$$2(1-\cos\xi)\Delta V_{R_2}^2 + na\Delta\delta\lambda(1-\cos\xi)\Delta V_{R_2} + n^2a^2(\Delta\delta\lambda^2/4 - (\Delta\delta e_x^2 + \Delta\delta e_y^2)) = 0 \tag{13}$$

$$2\Delta V_{R_2}^2 + na\Delta\delta\lambda\Delta V_{R_2} + \frac{n^2a^2}{(1-\cos\xi)}(\Delta\delta\lambda^2/4 - (\Delta\delta e_x^2 + \Delta\delta e_y^2)) = 0 \tag{14}$$

By solving Eq. (14), ΔV_{R_2} can be finally obtained as a function of ξ:

$$\Delta V_{R_2} = \frac{-na\Delta\delta\lambda \pm na\sqrt{\Delta\delta\lambda^2 - \frac{1}{(1-\cos\xi)}(2\Delta\delta\lambda^2 - 8(\Delta\delta e_x^2 + \Delta\delta e_y^2))}}{4} \tag{15}$$

Considering case b first, the condition of $\Delta\delta\lambda$ can be deduced by

$$\sqrt{\Delta\delta\lambda^2 - \frac{1}{(1-\cos\xi)}(2\Delta\delta\lambda^2 - 8\|\Delta\delta\boldsymbol{e}\|^2)} \le \Delta\delta\lambda \tag{16}$$

Since $(1-\cos\xi) \ge 0$, Eq. (16) leads to

$$\Delta\delta\lambda^2 \ge 4\|\Delta\delta\boldsymbol{e}\|^2 \tag{17}$$

In short, $J = \frac{na\Delta\delta\lambda}{2}$ when $\Delta\delta\lambda^2 \ge 4\|\Delta\delta\boldsymbol{e}\|^2$, regardless of the u and ξ values. Thus, there are infinite solutions available. Here, we assume $\xi = \pi$; then, the other variables are automatically decided as follows:

$$\Delta V_{R_2} = \frac{-na\Delta\delta\lambda \pm 2na\|\Delta\delta\boldsymbol{e}\|}{4}, \quad \Delta V_{R_1} = \frac{-na\Delta\delta\lambda \mp 2na\|\Delta\delta\boldsymbol{e}\|}{4} \tag{18}$$

From Eq. (4),

$$\begin{aligned} a\Delta\delta e_x &= \Delta V_{R_1}\sin u/n - \Delta V_{R_2}\sin u/n = \mp a\|\Delta\delta\boldsymbol{e}\|\sin u \\ a\Delta\delta e_y &= -\Delta V_{R_1}\cos u/n + \Delta V_{R_2}\cos u/n = \pm a\|\Delta\delta\boldsymbol{e}\|\cos u \\ \therefore u &= \tan^{-1}(-\Delta\delta e_x/\Delta\delta e_y) \end{aligned} \tag{19}$$

There are two combinations of $(\Delta V_{R_1}, \Delta V_{R_2})$ available, depending on u. If u is selected to make $\sin u$ as $(-\Delta\delta e_x/\|\Delta\delta\boldsymbol{e}\|)$ and $\cos u$ as $(\Delta\delta e_y/\|\Delta\delta\boldsymbol{e}\|)$, then $(\Delta V_{R_1}, \Delta V_{R_2})$ become

$$\Delta V_{R_1} = \frac{-na\Delta\delta\lambda - 2na\|\Delta\delta\boldsymbol{e}\|}{4}, \quad \Delta V_{R_2} = \frac{-na\Delta\delta\lambda + 2na\|\Delta\delta\boldsymbol{e}\|}{4} \tag{20}$$

When $\Delta\delta\lambda^2 < 4\|\Delta\delta\boldsymbol{e}\|^2$, on the other hand,

$$\Delta V_{R_2} = \frac{-na\Delta\delta\lambda + na\sqrt{\Delta\delta\lambda^2 - \frac{1}{(1-\cos\xi)}(2\Delta\delta\lambda^2 - 8\|\Delta\delta\boldsymbol{e}\|^2)}}{4} > 0$$

holds, and this indicates case c. For this case, the cost function can be redefined as a function of $\Delta\delta\boldsymbol{e}$ and ξ:

$$J = \frac{na\Delta\delta\lambda}{2} + 2\Delta V_{R_2} = \frac{na}{2}\sqrt{\Delta\delta\lambda^2 - \frac{1}{(1-\cos\xi)}(2\Delta\delta\lambda^2 - 8\|\Delta\delta\boldsymbol{e}\|^2)} \tag{21}$$

The partial derivative of J with respect to ξ can be obtained by

$$\frac{\partial J}{\partial\xi} = \frac{na}{4}\left(\Delta\delta\lambda^2 - \frac{1}{(1-\cos\xi)}(2\Delta\delta\lambda^2 - 8\|\Delta\delta\boldsymbol{e}\|^2)\right)^{-(1/2)} \times \frac{(2\Delta\delta\lambda^2 - 8\|\Delta\delta\boldsymbol{e}\|^2)}{(1-\cos\xi)^2}\sin\xi \tag{22}$$

Since $\Delta\delta\lambda^2 < 4\|\Delta\delta\boldsymbol{e}\|^2$, from the definition of case c, $(2\Delta\delta\lambda^2 - 8\|\Delta\delta\boldsymbol{e}\|^2)$ becomes negative. By defining C_0,

$$C_0 = C_0(\xi) \equiv \frac{na}{4}\left(\Delta\delta\lambda^2 - \frac{1}{(1-\cos\xi)}(2\Delta\delta\lambda^2 - 8\|\Delta\delta\boldsymbol{e}\|^2)\right)^{-(1/2)} \times \frac{(2\Delta\delta\lambda^2 - 8\|\Delta\delta\boldsymbol{e}\|^2)}{(1-\cos\xi)^2} > 0 \tag{23}$$

$\partial J/\partial\xi$ can be simplified as

$$\frac{\partial J}{\partial\xi} = -C_0\sin\xi \tag{24}$$

According to Eq. (24), J becomes the minimum when $\xi = \pi$, and the minimum value is found by

$$\begin{aligned} J|_{\xi=\pi} &= \frac{na}{2}\sqrt{\Delta\delta\lambda^2 - (\Delta\delta\lambda^2 - 4\|\Delta\delta\boldsymbol{e}\|^2)} \\ &= \frac{na}{2}\times 2\|\Delta\delta\boldsymbol{e}\| = na\|\Delta\delta\boldsymbol{e}\| \end{aligned} \tag{25}$$

The corresponding ΔV_{R_1} and ΔV_{R_2} can then be easily achieved by

$$\Delta V_{R_2} = \frac{-na\Delta\delta\lambda + 2na\|\Delta\delta\boldsymbol{e}\|}{4} = -\frac{na}{4}\Delta\delta\lambda + \frac{na}{2}\|\Delta\delta\boldsymbol{e}\| \tag{26}$$

$$\begin{aligned} \Delta V_{R_1} &= -\frac{na}{2}\Delta\delta\lambda - \left(\frac{-na\Delta\delta\lambda + 2na\|\Delta\delta\boldsymbol{e}\|}{4}\right) \\ &= -\frac{na}{4}\Delta\delta\lambda - \frac{na}{2}\|\Delta\delta\boldsymbol{e}\| \end{aligned} \tag{27}$$

Finally, the last unknown variable u can be obtained by

$$\begin{aligned} na\Delta\delta e_x &= \Delta V_{R_1}\sin u - \Delta V_{R_2}\sin u = -na\|\Delta\delta\boldsymbol{e}\|\sin u \\ na\Delta\delta e_y &= -\Delta V_{R_1}\cos u + \Delta V_{R_2}\cos u = na\|\Delta\delta\boldsymbol{e}\|\cos u \\ \therefore u &= \tan^{-1}(-\Delta\delta e_x/\Delta\delta e_y) \end{aligned} \tag{28}$$

Third, case a has the same solution as case c but with the switched $(\Delta V_{R_1}, \Delta V_{R_2})$ and different u:

$$\begin{aligned} &\Delta V_{R_2} = -\frac{na}{4}\Delta\delta\lambda - \frac{na}{2}\|\Delta\delta\boldsymbol{e}\|, \quad \Delta V_{R_1} = -\frac{na}{4}\Delta\delta\lambda + \frac{na}{2}\|\Delta\delta\boldsymbol{e}\| \\ &\sin u = (\Delta\delta e_x/\|\Delta\delta\boldsymbol{e}\|), \qquad \cos u = (-\Delta\delta e_y/\|\Delta\delta\boldsymbol{e}\|) \end{aligned} \tag{29}$$

Because u is the same as the previous one with only the phase difference of π, Eq. (29) for case a is eventually identical to the solution of cases b and c.

Lastly, if $\cos\xi = 1$, Eq. (4) can be written as follows:

$$\begin{aligned} a\Delta\delta\lambda &= -2\Delta V_{R_1}/n - 2\Delta V_{R_2}/n = -2(\Delta V_{R_1} + \Delta V_{R_2})/n \\ a\Delta\delta e_x &= \Delta V_{R_1}\sin u/n + \Delta V_{R_2}\sin u/n \\ &= (\Delta V_{R_1} + \Delta V_{R_2})/n \times \sin u \\ a\Delta\delta e_y &= -\Delta V_{R_1}\cos u/n - \Delta V_{R_2}\cos u/n \\ &= -(\Delta V_{R_1} + \Delta V_{R_2})/n \times \cos u \end{aligned} \tag{30}$$

where $u = \tan^{-1}(-\Delta\delta e_x/\Delta\delta e_y)$. Note that, however, Eq. (30) does not have a solution if $\Delta\delta\lambda/2 \ne \Delta\delta e_y/\cos u = \|\Delta\delta\boldsymbol{e}\|$; otherwise, the first and the third equations in Eq. (30) will be parallel. In other words, there will be no possible $(\Delta V_{R_1}, \Delta V_{R_2})$ combination that satisfies

required $(\Delta\delta e_x, \Delta\delta e_y)$. There will be an infinite number of solutions when $\Delta\delta\lambda/2 = \|\Delta\delta\boldsymbol{e}\|$ since Eq. (30) is underdetermined. In this case, any $(\Delta V_{R_1}, \Delta V_{R_2})$ that satisfy $-\frac{na\Delta\delta\lambda}{2} \le \Delta V_{R_2} \le 0$ minimize J as $J = \frac{na\Delta\delta\lambda}{2}$. The solutions for the three cases are summarized in Table 1.

IV. In-Plane Reconfiguration with Three Radial Maneuvers

In-plane relative orbit change by three radial impulses ΔV_{R_1}, ΔV_{R_2}, and ΔV_{R_3} is derived as follows. There are now three equations with six unknown variables: ΔV_{R_1}, ΔV_{R_2}, ΔV_{R_3}, u_1, u_2, and u_3:

$$
\begin{aligned}
a\Delta\delta\lambda &= -2\Delta V_{R_1}/n - 2\Delta V_{R_2}/n - 2\Delta V_{R_3}/n \\
a\Delta\delta e_x &= \Delta V_{R_1}\sin u_1/n + \Delta V_{R_2}\sin u_2/n + \Delta V_{R_3}\sin u_3/n \\
a\Delta\delta e_y &= -\Delta V_{R_1}\cos u_1/n - \Delta V_{R_2}\cos u_2/n - \Delta V_{R_3}\cos u_3/n
\end{aligned} \tag{31}
$$

If u_1, u_2, and u_3 are defined as $(u + k_i\pi)$ with integer k_i, then the equations can be simplified by

$$
\begin{aligned}
na\Delta\delta\lambda &= -2\Delta V_{R_1} - 2\Delta V_{R_2} - 2\Delta V_{R_3} \\
na\Delta\delta e_x &= (-1)^{k_1}\times\Delta V_{R_1}\sin u + (-1)^{k_2} \\
&\quad \times\Delta V_{R_2}\sin u + (-1)^{k_3}\times\Delta V_{R_1}\sin u \\
na\Delta\delta e_y &= -(-1)^{k_1}\times\Delta V_{R_1}\cos u - (-1)^{k_2} \\
&\quad \times\Delta V_{R_2}\cos u - (-1)^{k_3}\times\Delta V_{R_3}\cos u
\end{aligned} \tag{32}
$$

Now, there are seven unknown variables: ΔV_{R_1}, ΔV_{R_2}, ΔV_{R_3}, u, k_1, k_2 and k_3. To reduce the number of variables, u is assumed to be the same as Eqs. (19) and (28) in the two-impulse case such that

$$
\Delta\delta e_x/\Delta\delta e_y = -\sin u/\cos u \quad \therefore u = \tan^{-1}(-\Delta\delta e_x/\Delta\delta e_y) \tag{33}
$$

There are six cases according to the set of integers (k_1, k_2, k_3). In the following, we introduce an example process of deriving the local minimum impulse solution under $u_i = (u + k_i\pi)$. Only the first two combinations are introduced, whereas the complete solution is summarized in Table 2:

Case a: $k_1 = 2l$, $k_2 = 2m$, $k_3 = 2n$

$$
\begin{aligned}
na\Delta\delta\lambda &= -2\Delta V_{R_1} - 2\Delta V_{R_2} - 2\Delta V_{R_3} \\
na\Delta\delta e_x &= \Delta V_{R_1}\sin u + \Delta V_{R_2}\sin u + \Delta V_{R_3}\sin u \\
na\Delta\delta e_y &= -\Delta V_{R_1}\cos u - \Delta V_{R_2}\cos u - \Delta V_{R_3}\cos u
\end{aligned} \tag{34}
$$

From Eq. (34), $(\Delta V_{R_1} + \Delta V_{R_2} + \Delta V_{R_3})$ can be written in a different form:

$$
\begin{aligned}
na\Delta\delta e_x\sin u &= (\Delta V_{R_1} + \Delta V_{R_2} + \Delta V_{R_3})\sin^2 u \\
na\Delta\delta e_y\cos u &= (-\Delta V_{R_1} - \Delta V_{R_2} - \Delta V_{R_3})\cos^2 u \\
\Delta V_{R_1} + \Delta V_{R_2} + \Delta V_{R_3} &= na\Delta\delta e_x\sin u - na\Delta\delta e_y\cos u
\end{aligned} \tag{35}
$$

We can easily see that there is no solution if $-\Delta\delta\lambda/2 \ne \Delta\delta e_x\sin u - \Delta\delta e_y\cos u$:

Case b: $k_1 = 2l$, $k_2 = 2m$, $k_3 = 2n + 1$

$$
\begin{aligned}
na\Delta\delta\lambda &= -2\Delta V_{R_1} - 2\Delta V_{R_2} - 2\Delta V_{R_3} \\
na\Delta\delta e_x &= \Delta V_{R_1}\sin u + \Delta V_{R_2}\sin u - \Delta V_{R_3}\sin u \\
na\Delta\delta e_y &= -\Delta V_{R_1}\cos u - \Delta V_{R_2}\cos u + \Delta V_{R_3}\cos u
\end{aligned} \tag{36}
$$

Since ΔV_{R_3} has a different sign in Eq. (36),

$$
\begin{aligned}
\Delta V_{R_1} + \Delta V_{R_2} + \Delta V_{R_3} &= -na\Delta\delta\lambda/2 \\
na\Delta\delta e_x &= (-na\Delta\delta\lambda/2)\sin u - 2\Delta V_{R_3}\sin u \\
na\Delta\delta e_y &= -(-na\Delta\delta\lambda/2)\cos u + 2\Delta V_{R_3}\cos u
\end{aligned} \tag{37}
$$

$(\Delta V_{R_1} + \Delta V_{R_2} - \Delta V_{R_3})$ can be derived as follows:

$$
\begin{aligned}
na\Delta\delta e_x\sin u &= (\Delta V_{R_1} + \Delta V_{R_2} - \Delta V_{R_3})\sin^2 u \\
na\Delta\delta e_y\cos u &= (-\Delta V_{R_1} - \Delta V_{R_2} + \Delta V_{R_3})\cos^2 u \\
\Delta V_{R_1} + \Delta V_{R_2} - \Delta V_{R_3} &= na\Delta\delta e_x\sin u - na\Delta\delta e_y\cos u
\end{aligned} \tag{38}
$$

From $\Delta\delta\lambda$ in Eqs. (36) and (38), ΔV_{R_3} can be obtained by

$$
\begin{aligned}
&\Delta V_{R_1} + \Delta V_{R_2} + \Delta V_{R_3} = -na\Delta\delta\lambda/2 \\
&na\Delta\delta e_x\sin u - na\Delta\delta e_y\cos u = \Delta V_{R_1} + \Delta V_{R_2} - \Delta V_{R_3} \\
&\quad = (-na\Delta\delta\lambda/2) - 2\Delta V_{R_3} \\
&\therefore \Delta V_{R_3} = -\frac{1}{2}na\Delta\delta e_x\sin u + \frac{1}{2}na\Delta\delta e_y\cos u - \frac{1}{4}na\Delta\delta\lambda
\end{aligned} \tag{39}
$$

From Eq. (39), $(\Delta V_{R_1} + \Delta V_{R_2})$ can be found by

$$
\Delta V_{R_1} + \Delta V_{R_2} = \frac{1}{2}na\Delta\delta e_x\sin u - \frac{1}{2}na\Delta\delta e_y\cos u - \frac{1}{4}na\Delta\delta\lambda \tag{40}
$$

Table 1 Two radial maneuvers' solution for in-plane reconfiguration

	Minimum impulses solution	$\sum\lvert\Delta V_{R_i}\rvert$
$\Delta\delta\lambda^2 > 4\lVert\Delta\delta\boldsymbol{e}\rVert^2$	Infinite solutions with respect to u_1 selection, and one of them could be $\Delta V_{R_1} = -\frac{na}{4}\Delta\delta\lambda - \frac{na}{2}\lVert\Delta\delta\boldsymbol{e}\rVert$, where $u_1 = \tan^{-1}(-\Delta\delta e_x/\Delta\delta e_y)$, and $\Delta V_{R_2} = -\frac{na}{4}\Delta\delta\lambda + \frac{na}{2}\lVert\Delta\delta\boldsymbol{e}\rVert$, where $u_2 = u_1 + \pi$	$\frac{na\Delta\delta\lambda}{2}$
$\Delta\delta\lambda^2 = 4\lVert\Delta\delta\boldsymbol{e}\rVert^2$	Infinite solutions with respect to u_1 selection, and one of them could be $\Delta V_{R_1} = -\frac{na}{4}\Delta\delta\lambda - \frac{na}{2}\lVert\Delta\delta\boldsymbol{e}\rVert$, where $u_1 = \tan^{-1}(-\Delta\delta e_x/\Delta\delta e_y)$, and $\Delta V_{R_2} = -\frac{na}{4}\Delta\delta\lambda + \frac{na}{2}\lVert\Delta\delta\boldsymbol{e}\rVert$, where $u_2 = u_1 + \pi$ Also, $u_2 = u_1 + 2\pi$ is available only with any $(\Delta V_{R_1}, \Delta V_{R_2})$ combination that satisfies $-\frac{na\Delta\delta\lambda}{2} \le \Delta V_{R_2} \le 0$, where $u_1 = \tan^{-1}(-\Delta\delta e_x/\Delta\delta e_y)$ and $\Delta V_{R_1} = -\frac{na\Delta\delta\lambda}{2} - \Delta V_{R_2}$	$\frac{na\Delta\delta\lambda}{2} = na\lVert\Delta\delta\boldsymbol{e}\rVert$
$\Delta\delta\lambda^2 < 4\lVert\Delta\delta\boldsymbol{e}\rVert^2$	$\Delta V_{R_1} = -\frac{na}{4}\Delta\delta\lambda - \frac{na}{2}\lVert\Delta\delta\boldsymbol{e}\rVert$, where $u_1 = \tan^{-1}(-\Delta\delta e_x/\Delta\delta e_y)$, and $\Delta V_{R_2} = -\frac{na}{4}\Delta\delta\lambda + \frac{na}{2}\lVert\Delta\delta\boldsymbol{e}\rVert$, where $u_2 = u_1 + \pi$	$na\lVert\Delta\delta\boldsymbol{e}\rVert$

Table 2 Three radial maneuvers' solution for in-plane reconfiguration

Sign $(-1)^{k_i}$	Local minimum impulses solution when $u_i = (u + k_i\pi)$	$\sum \lvert\Delta V_{R_i}\rvert$
$+++$	There is no solution if $-\Delta\delta\lambda/2 \neq \Delta\delta e_x \sin u - \Delta\delta e_y \cos u$.	— —
$---$	There is no solution if $-\Delta\delta\lambda/2 \neq -\Delta\delta e_x \sin u + \Delta\delta e_y \cos u$.	— —
$+--$	$\Delta V_{R_1} = \frac{1}{2}na\Delta\delta e_x \sin u - \frac{1}{2}na\Delta\delta e_y \cos u - \frac{1}{4}na\Delta\delta\lambda$ $\lvert\Delta V_{R_2}\rvert + \lvert\Delta V_{R_3}\rvert = \lvert\Delta V_{R_2} + \Delta V_{R_3}\rvert$, and one possible solution is $\Delta V_{R_2} = \Delta V_{R_3} = -\frac{1}{4}na\Delta\delta e_x \sin u + \frac{1}{4}na\Delta\delta e_y \cos u - \frac{1}{8}na\Delta\delta\lambda$	
$-++$	$\Delta V_{R_1} = -\frac{1}{2}na\Delta\delta e_x \sin u + \frac{1}{2}na\Delta\delta e_y \cos u - \frac{1}{4}na\Delta\delta\lambda$ $\lvert\Delta V_{R_2}\rvert + \lvert\Delta V_{R_3}\rvert = \lvert\Delta V_{R_2} + \Delta V_{R_3}\rvert$, and one possible solution is $\Delta V_{R_2} = \Delta V_{R_3} = \frac{1}{4}na\Delta\delta e_x \sin u - \frac{1}{4}na\Delta\delta e_y \cos u - \frac{1}{8}na\Delta\delta\lambda$	
$+-+$	$\Delta V_{R_2} = -\frac{1}{2}na\Delta\delta e_x \sin u + \frac{1}{2}na\Delta\delta e_y \cos u - \frac{1}{4}na\Delta\delta\lambda$ $\lvert\Delta V_{R_1}\rvert + \lvert\Delta V_{R_3}\rvert = \lvert\Delta V_{R_1} + \Delta V_{R_3}\rvert$, and one possible solution is $\Delta V_{R_1} = \Delta V_{R_3} = \frac{1}{4}na\Delta\delta e_x \sin u - \frac{1}{4}na\Delta\delta e_y \cos u - \frac{1}{8}na\Delta\delta\lambda$	$\frac{na\Delta\delta\lambda}{2}$, where $\Delta\delta\lambda^2 \geq 4\lVert\Delta\delta\boldsymbol{e}\rVert^2$
$-+-$	$\Delta V_{R_2} = \frac{1}{2}na\Delta\delta e_x \sin u - \frac{1}{2}na\Delta\delta e_y \cos u - \frac{1}{4}na\Delta\delta\lambda$ $\lvert\Delta V_{R_1}\rvert + \lvert\Delta V_{R_3}\rvert = \lvert\Delta V_{R_1} + \Delta V_{R_3}\rvert$, and one possible solution is $\Delta V_{R_1} = \Delta V_{R_3} = -\frac{1}{4}na\Delta\delta e_x \sin u + \frac{1}{4}na\Delta\delta e_y \cos u - \frac{1}{8}na\Delta\delta\lambda$	$na\lvert\Delta\delta e_x \sin u - \Delta\delta e_y \cos u\rvert$ $= na\lvert\Delta\delta e_x \frac{-\Delta\delta e_x}{\lVert\Delta\delta\boldsymbol{e}\rVert} - \Delta\delta e_y \frac{\Delta\delta e_y}{\lVert\Delta\delta\boldsymbol{e}\rVert}\rvert$ $= na\lVert\Delta\delta\boldsymbol{e}\rVert$, where $\Delta\delta\lambda^2 < 4\lVert\Delta\delta\boldsymbol{e}\rVert^2$
$++-$	$\Delta V_{R_3} = -\frac{1}{2}na\Delta\delta e_x \sin u + \frac{1}{2}na\Delta\delta e_y \cos u - \frac{1}{4}na\Delta\delta\lambda$ $\lvert\Delta V_{R_1}\rvert + \lvert\Delta V_{R_2}\rvert = \lvert\Delta V_{R_1} + \Delta V_{R_2}\rvert$, and one possible solution is $\Delta V_{R_1} = \Delta V_{R_2} = \frac{1}{4}na\Delta\delta e_x \sin u - \frac{1}{4}na\Delta\delta e_y \cos u - \frac{1}{8}na\Delta\delta\lambda$	
$--+$	$\Delta V_{R_3} = \frac{1}{2}na\Delta\delta e_x \sin u - \frac{1}{2}na\Delta\delta e_y \cos u - \frac{1}{4}na\Delta\delta\lambda$ $\lvert\Delta V_{R_1}\rvert + \lvert\Delta V_{R_2}\rvert = \lvert\Delta V_{R_1} + \Delta V_{R_2}\rvert$, and one possible solution is $\Delta V_{R_1} = \Delta V_{R_2} = -\frac{1}{4}na\Delta\delta e_x \sin u + \frac{1}{4}na\Delta\delta e_y \cos u - \frac{1}{8}na\Delta\delta\lambda$	

For Eq. (40), $|\Delta V_{R_1}| + |\Delta V_{R_2}|$ is minimized when $|\Delta V_{R_1}| + |\Delta V_{R_2}| = |\Delta V_{R_1} + \Delta V_{R_2}|$. One possible solution can be selected as follows, which corresponds to the $++-$ combination in Table 2:

$$\Delta V_{R_1} = \Delta V_{R_2} = \frac{1}{4}na\Delta\delta e_x \sin u - \frac{1}{4}na\Delta\delta e_y \cos u - \frac{1}{8}na\Delta\delta\lambda \quad (41)$$

Although $\sum |\Delta V_{R_i}|$ is equivalent to those in Table 1, three impulsive maneuvers could be still useful since each of ΔV_{R_i} can be smaller. In other words, more ΔV_{R_i} combinations can be available under the same delta-v limit of the propulsion system.

V. Examples of In-Plane Reconfigurations

Numerical results are presented to verify the proposed two- and three-radial-impulsive solutions. Figure 1 shows the flowchart applied in the simulation. First, the orbits of both satellites are propagated in the inertial frame. Then, they are converted into the mean OEs [21], and the mean ROE are obtained from the two mean

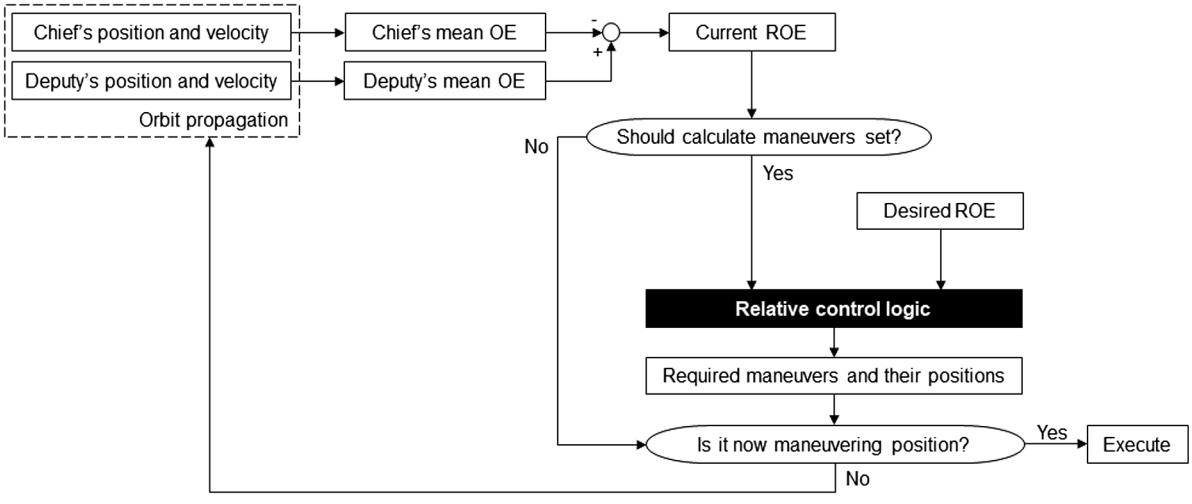

Fig. 1 Simulation study configuration.

Table 3 Relative orbit reconfiguration scenario 1

Initial reference orbit					
a, km	e	i, deg	Ω, deg	ω, deg	$M(0)$, deg
6928	0.002	98	0	45	0
Initial relative orbit elements					
$a\delta a$, m	$a\delta e_x$, m	$a\delta e_y$, m	$a\delta i_x$, m	$a\delta i_y$, m	$a\delta\lambda$, m
0	0	0	0	0	0
Desired relative orbit elements					
$a\delta a$, m	$a\delta e_x$, m	$a\delta e_y$, m	$a\delta i_x$, m	$a\delta i_y$, m	$a\delta\lambda$, m
0	0	15	0	−15	0

OEs. After calculating the required impulsive solutions, they are applied as delta-v in the inertial frame during propagation.

A. $\Delta\delta\lambda = 0$

Initial reference OE of the chief satellite is given in Table 3, whereas initial ROE of the deputy satellite is set to zero. Desired ROE is assumed as the 15 m helix orbit [8] without the along-track offset: $\Delta\delta\lambda = 0$. The J2 disturbance is included during orbit propagation, and it is considered in the ΔV calculation by using the state transition matrix presented in Ref. [22].

The two-impulse solution is summarized in Table 4. We can see that the delta-v magnitudes are the same since $\Delta\delta\lambda = 0$, shown by Eq. (18).

The three-impulse solution is obtained from the same problem and summarized in Table 5. For comparison, the previous three-tangential-impulse method is also applied for reconfiguration [10]. The fastest reconfiguration scenario is assumed for the tangential maneuver case ($k_1 = 0, k_2 = 1, k_3 = 2$). The results demonstrate that the tangential maneuver solution is twice as efficient for relative eccentricity vector control, as can be inferred by the dynamics in Eq. (2).

To verify whether $\sum|\Delta V_i|$ remains the same with other $(\Delta V_{R_1}, \Delta V_{R_3})$ combinations (mathematically proven in Table 2) as long as $|\Delta V_{R_1}| + |\Delta V_{R_3}| = |\Delta V_{R_1} + \Delta V_{R_3}|$ is satisfied, another $(\Delta V_{R_1}, \Delta V_{R_3})$ is applied, and its results are summarized in Table 6. It can be seen that the total amount of delta-v $\sum|\Delta V_i|$ is the same as expected.

B. $\Delta\delta\lambda \neq 0$: Case b $\Delta\delta\lambda^2 \geq 4\|\Delta\delta e\|^2$

Table 7 shows a new reconfiguration scenario with the 300 m along-track offset. This condition corresponds to case b. A two-impulse solution is first obtained, and its results are summarized in Table 8. Compared to the results of $\Delta\delta\lambda = 0$, it is shown that the total delta-v is greatly increased. To verify whether $\sum|\Delta V_i|$ remains the same regardless of the maneuver positions, the different initial impulse position ($u_1 = 60$ deg) is adopted, and its results are summarized in Table 9. Three-impulse solutions in radial and tangential directions are summarized in Table 10. Two remarks can be noted as follows. First, the benefit of increasing number of impulse in the radial maneuver method can be found. The maximum delta-v among the delta-v set is decreased from 0.0856 into 0.0739 m/s, which means that the less powerful thruster can be employed for the same reconfiguration scenario. Second, the disadvantage of the radial

Table 4 Two radial maneuvers' result from reconfiguration scenario 1

Parameter	Value
u_1, rad	0
u_2, rad	3.1416
ΔV_{R_1}, m/s	−0.0082
ΔV_{R_2}, m/s	0.0082
$\sum\|\Delta V_{R_i}\|$, m/s	0.0164

Table 6 Three radial maneuvers' result from reconfiguration scenario 1 with different delta-V combinations

Parameter	Value
ΔV direction	Radial
u_1, rad	0
u_2, rad	3.1416
u_3, rad	6.2832
ΔV_1, m/s	−0.0062
ΔV_2, m/s	−0.0082
ΔV_3, m/s	−0.0021
$\sum\|\Delta V_i\|$, m/s	0.0164

Table 7 Relative orbit reconfiguration scenario 2: case b

Desired relative orbit elements	Values
$a\delta a$, m	0
$a\delta e_x$, m	0
$a\delta e_y$, m	15
$a\delta i_x$, m	0
$a\delta i_y$, m	−15
$a\delta\lambda$, m	300

Table 8 Two radial maneuvers' result from reconfiguration scenario 2

Parameter	Value
u_1, rad	0
u_2, rad	3.1416
ΔV_{R_1}, m/s	−0.0903
ΔV_{R_2}, m/s	−0.0739
$\sum\|\Delta V_{R_i}\|$, m/s	0.1642

Table 9 Two radial maneuvers' result for reconfiguration scenario 2 ($u_1 = 60$ deg)

Parameter	Value
u_1, rad	1.0472
u_2, rad	4.3706
ΔV_{R_1}, m/s	−0.0856
ΔV_{R_2}, m/s	−0.0787
$\sum\|\Delta V_{R_i}\|$, m/s	0.1642

Table 5 Three radial (top) and tangential (bottom) maneuvers' result from reconfiguration scenario 1

ΔV direction	u_1, rad	u_2, rad	u_3, rad	ΔV_1, m/s	ΔV_2, m/s	ΔV_3, m/s	$\sum\|\Delta V_i\|$, m/s
Radial	0	3.1416	6.2832	−0.0041	−0.0082	−0.0041	0.0164
Tangential	1.5708	4.7124	7.8540	0.0021	−0.0041	0.0021	0.0082

Table 10 Three radial (top) and tangential (bottom) maneuvers' result from reconfiguration scenario 2

ΔV direction	u_1, rad	u_2, rad	u_3, rad	ΔV_1, m/s	ΔV_2, m/s	ΔV_3, m/s	$\sum \lvert\Delta V_i\rvert$, m/s
Radial	0	3.1416	6.2832	−0.0452	−0.0739	−0.0452	0.1642
Tangential	1.5708	4.7124	7.8540	−0.0154	−0.0041	0.0195	0.0390

Table 11 Relative orbit reconfiguration scenario 3: case a or c

Desired relative orbit elements	Values
$a\delta a$, m	0
$a\delta e_x$, m	0
$a\delta e_y$, m	15
$a\delta i_x$, m	0
$a\delta i_y$, m	−15
$a\delta\lambda$, m	20

maneuver approach with respect to fuel efficiency can be clearly seen. One possible remedy would be the use of differential drag control to adjust the along-track distance $a\Delta\delta\lambda$ until $\Delta\delta\lambda^2 < 4\|\Delta\delta\boldsymbol{e}\|^2$ holds.

C. $\Delta\delta\lambda \neq 0$: Case a or c $\Delta\delta\lambda^2 < 4\|\Delta\delta\boldsymbol{e}\|^2$

The along-track distance is adjusted to 20 m, as in Table 11, which conforms the $\Delta\delta\lambda^2 < 4\|\Delta\delta\boldsymbol{e}\|^2$ condition. A two-impulse solution is summarized in Table 12. We can see that the total delta-v cost is equivalent to that of the $\Delta\delta\lambda = 0$ condition, which verifies that the delta-v cost is independent of $\Delta\delta\lambda$ when $\Delta\delta\lambda^2 < 4\|\Delta\delta\boldsymbol{e}\|^2$ holds. Compared to case b, the delta-v cost is now dependent on the impulse firing positions, and it can be seen by comparing the results in Tables 12 and 13. Finally, double fuel efficiency of the tangential-impulsive-solution compared to the proposed radial-impulsive-solution can be found in Table 14.

Table 12 Two radial maneuvers' result for reconfiguration scenario 3

Parameter	Value
u_1, rad	0
u_2, rad	3.1416
ΔV_{R_1}, m/s	−0.0137
ΔV_{R_2}, m/s	0.0027
$\sum \lvert\Delta V_{R_i}\rvert$, m/s	0.0164

Table 13 Two radial maneuvers' result for reconfiguration scenario 3 ($u_1 = 60$ deg)

Parameter	Value
u_1, rad	1.0472
u_2, rad	6.9501
ΔV_{R_1}, m/s	0.0274
ΔV_{R_2}, m/s	−0.0383
$\sum \lvert\Delta V_{R_i}\rvert$, m/s	0.0657

Table 15 Relative orbit reconfiguration scenario 4 (sequential)

$a\delta a$, m	$a\delta e_x$, m	$a\delta e_y$, m	$a\delta i_x$, m	$a\delta i_y$, m	$a\delta\lambda$, m
Initial relative orbit elements					
0	0	0	0	0	0
Desired relative orbit elements 1					
0	0	15	0	−15	0
Desired relative orbit elements 2					
0	0	20	0	−20	300
Desired relative orbit elements 3					
0	0	10	0	−10	200

Table 16 Simulation condition for scenario 4

Parameter	Value
ΔV error (1 sigma)	1.5 % of ΔV_i
Reconfiguration time window	2 orbits
Rest time between reconfigurations	17 orbits

D. Robustness Test Against Thrust Magnitude Error

In the last simulation case, thrust magnitude errors are incorporated into the delta-v commands in order to test the robustness of the reconfiguration methods. Both of the three radial- and tangential-impulsive methods are applied, and their performances are compared. The simulation case is defined by conducting the previous three reconfiguration maneuvers sequentially as shown in Table 15, from the initial ROE to the final ROE (i.e., ROE0 to ROE3). It is assumed that the only one reconfiguration maneuver from ROE1 to ROE2 is corrupted by the thrust errors so that ROE3 can be exactly achieved at the end. The thrust error is assumed to be proportional to the delta-v magnitude (i.e., scale factor error) [16], and it follows the Gaussian distribution function with zero mean and 0.015 standard deviations (i.e., 1.5%), as in Table 16. The rest time between each reconfiguration is set to 17 orbits, where the secular drift motion due to the thrust error can be observed. For the out-of-plane maneuver, single ΔV_N is applied the same as the one used in the previous studies, e.g., in Ref. [10].

Figures 2 and 3 show the resultant relative motion represented in the Cartesian coordinate frame. The along-track drift motion after the second reconfiguration maneuver (i.e., ROE1 to ROE2) in the tangential maneuver case can be clearly seen. It is mainly caused by the relative SMA control error. While the desired along-track offset $a\Delta\delta\lambda$ is 300 m and is supposed to be kept constant, it drifts over time and even approaches to the $a\Delta\delta\lambda = 0$ condition. This condition can adversely affect the safety condition when the e/i vector separation

Table 14 Three radial (top) and tangential (bottom) maneuvers' result from reconfiguration scenario 3

ΔV direction	u_1, rad	u_2, rad	u_3, rad	ΔV_1, m/s	ΔV_2, m/s	ΔV_3, m/s	$\sum \lvert\Delta V_i\rvert$, m/s
Radial	0	3.1416	6.2832	−0.0068	0.0027	−0.0068	0.0164
Tangential	1.5708	4.7124	7.8540	0.0009	−0.0041	0.0032	0.0082

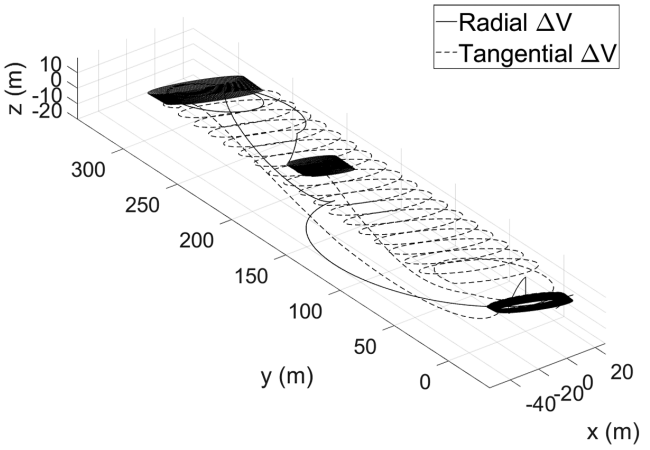

Fig. 2 Relative trajectory in Hill–Clohessy–Wiltshire (HCW) frame.

condition does not hold (i.e., $\delta \boldsymbol{e}$ is not parallel with $\delta \boldsymbol{i}$). On the other hand, in the radial maneuver case, the along-track control error is bounded since the relative SMA is not affected by the radial impulses.

Figures 4 and 5 represent the relative motion in the ROE parameterization. In Fig. 4, again, the along-track drift motion after the second reconfiguration maneuver can be observed. Figure 5 shows the other four ROE' histories, which are $a(\Delta\delta e_x, \Delta\delta e_y, \Delta\delta i_x, \Delta\delta i_y)$. Compared to the $\Delta\delta\lambda$ difference between the two maneuver methods, the control error differences in the relative eccentricity vector components $(\Delta\delta e_x, \Delta\delta e_y)$ are both small and bounded. The control error differences in $(\Delta\delta i_x, \Delta\delta i_y)$ are the same since the delta-v in the orbit-normal direction are equivalent to each other.

Table 17 summarizes the sets of the delta-v applied in the radial and tangential control methods. The total delta-v without the thrust error (i.e., ideal solution) are also shown in the last column. Note that the delta-v at the last reconfiguration (ROE2 to ROE3) are only changed since the thrust errors are only applied at the second reconfiguration. It can be easily seen that the thrust error increases the delta-v cost. The inaccurate completion of reconfiguration increases the delta-v cost at the following reconfiguration due to the ROE control errors. Noticeably, the increase of delta-v is larger with the tangential maneuver method because of the along-track drift motion. Specifically, the delta-v at the last reconfiguration in the tangential and radial maneuver approaches are increased by 55 and 7%, respectively.

VI. Sensitivity Analysis

In the previous section, the impact of the thrust error on the ROE control errors was observed by the numerical examples. In this section, the (worst-case) ROE control errors from the thrust error are systematically analyzed. Specifically, the three-impulse radial and tangential methods are focused on.

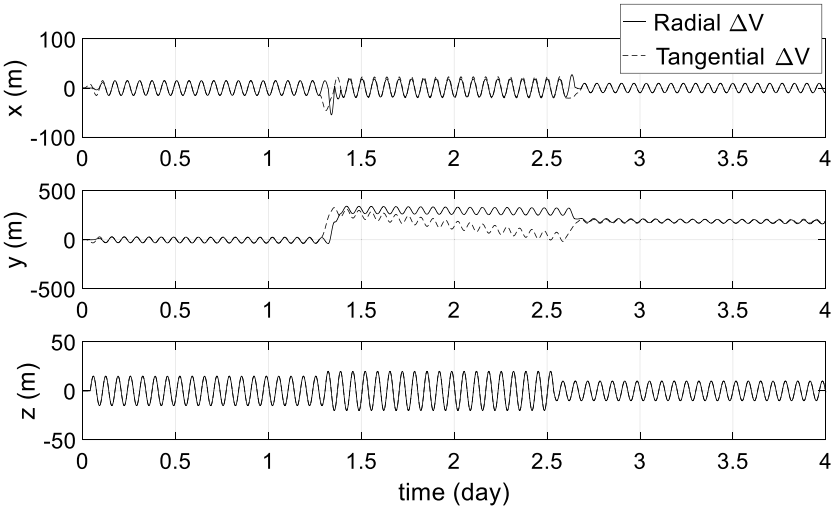

Fig. 3 Relative trajectory in HCW frame (in each axis).

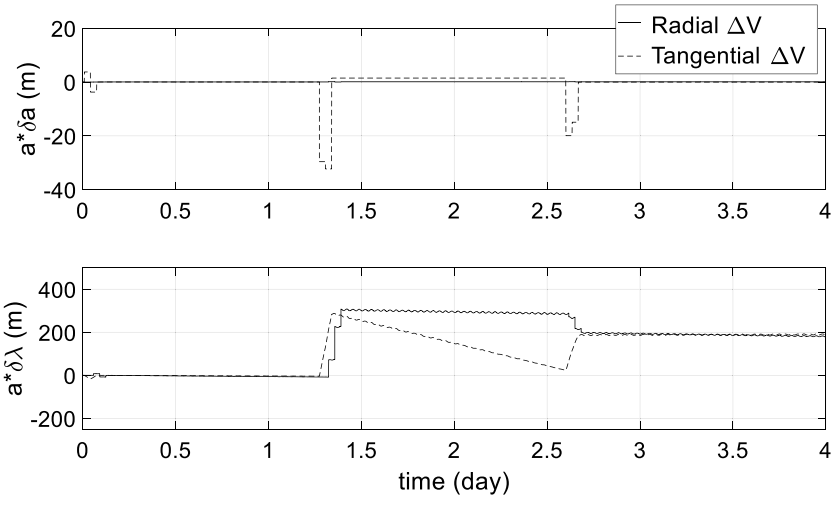

Fig. 4 Relative semimajor axis (top) and relative longitude (bottom) histories.

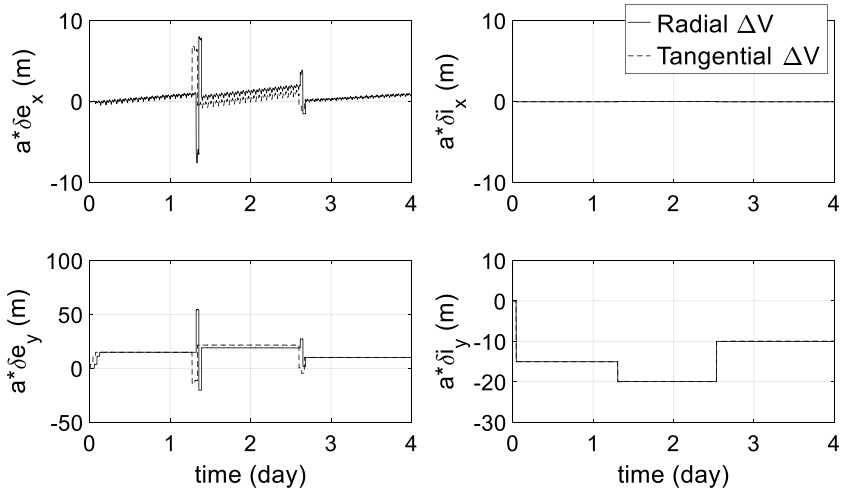

Fig. 5 Relative eccentricity vector (left) and relative inclination vector (right) histories.

A. In-Plane Reconfiguration with Three Radial Maneuvers

Random errors in the delta-v magnitudes are defined by

$$\begin{aligned}\Delta V_{R_1,\text{real}} &= (1+\alpha_1)\Delta V_{R_1}\\ \Delta V_{R_2,\text{real}} &= (1+\alpha_2)\Delta V_{R_2}\\ \Delta V_{R_3,\text{real}} &= (1+\alpha_3)\Delta V_{R_3}\end{aligned} \tag{42}$$

where the scale factor errors α_1, α_2, and α_3 feature Gaussian distribution with the same 3-sigma σ_α:

$$(\alpha_1,\alpha_2,\alpha_3) \propto N\left(0,\left(\frac{\sigma_\alpha}{3}\right)^2\right) \tag{43}$$

Case a: $\Delta\delta\lambda^2 < 4\|\Delta\delta\boldsymbol{e}\|^2$

Based on the three radial maneuver solutions in Table 2, the ROE errors caused by the thrust errors can be predicted. First, the relative eccentricity vector error $(\delta e_{x,\text{err}}, \delta e_{y,\text{err}})$ is derived. As an example, we first assume that $\Delta V_{R_1}, \Delta V_{R_2} < 0$ and $\Delta V_{R_3} > 0$, i.e., the $(++-)$ combination in Table 2:

$$na\delta e_{x,\text{err}} = (\alpha_1\Delta V_{R_1} + \alpha_2\Delta V_{R_2} - \alpha_3\Delta V_{R_3})\sin u \tag{44}$$

$$na\delta e_{y,\text{err}} = (-\alpha_1\Delta V_{R_1} - \alpha_2\Delta V_{R_2} + \alpha_3\Delta V_{R_3})\cos u \tag{45}$$

Defining a random parameter A as

$$A \equiv \alpha_1\Delta V_{R_1} + \alpha_2\Delta V_{R_2} - \alpha_3\Delta V_{R_3} \tag{46}$$

where

$$A \propto N\left(0,(\Delta V_{R_1}^2 + \Delta V_{R_2}^2 + \Delta V_{R_3}^2)\left(\frac{\sigma_\alpha}{3}\right)^2\right)$$

the estimated relative eccentricity error $\|\delta\boldsymbol{e}_{\text{err}}\| = \sqrt{\delta e_{x,\text{err}}^2 + \delta e_{y,\text{err}}^2}$ can be obtained by Eqs. (44) and (45) such that

$$n^2a^2\|\delta\boldsymbol{e}_{\text{err}}\|^2 = n^2a^2(\delta e_{x,\text{err}}^2 + \delta e_{y,\text{err}}^2) = A^2 \tag{47}$$

Then, we define the worst-case relative eccentricity error $\|\delta\boldsymbol{e}_{\text{err}}^*\|$, from the thrust error, by

$$\|\delta\boldsymbol{e}_{\text{err}}^*\| = |A|^*/na \tag{48}$$

where $|A|^*$ is the maximum expected value from the set of $(\alpha_1,\alpha_2,\alpha_3)$, which can be obtained by their 3-sigma values in Eq. (43) and the equation $na\|\Delta\delta\boldsymbol{e}\| = |\Delta V_{R_1}| + |\Delta V_{R_2}| + |\Delta V_{R_3}|$ in Table 2 such that

$$|A|^* = \sigma_\alpha na\|\Delta\delta\boldsymbol{e}\| \tag{49}$$

along with the maximum scale factor errors $(\alpha_1^*,\alpha_2^*,\alpha_3^*)$:

$$\begin{pmatrix}\alpha_1^*\\ \alpha_2^*\\ \alpha_3^*\end{pmatrix} = \begin{pmatrix}\pm\sigma_\alpha\\ \pm\sigma_\alpha\\ \pm\sigma_\alpha\end{pmatrix} \tag{50}$$

It can be easily shown that Eq. (50) also holds for the other combinations of signs of delta-v in Table 2. Then, the worst-case relative eccentricity error $\|\delta\boldsymbol{e}_{\text{err}}^*\|$ in Eq. (48) becomes

$$\|\delta\boldsymbol{e}_{\text{err}}^*\| = \sigma_\alpha\|\Delta\delta\boldsymbol{e}\| \tag{51}$$

Table 17 Three radial (top) and tangential (bottom) maneuvers' result from reconfiguration

ΔV direction		u_1, rad	u_2, rad	u_3, rad	ΔV_1, m/s	ΔV_2, m/s	ΔV_3, m/s	$\sum\|\Delta V_i\|$	$\sum\|\Delta V_i\|$ (without error)
Radial	1	0	3.1416	6.2832	−0.0041	0.0082	−0.0041	0.0164	0.0164
	2	119.554	122.696	125.837	−0.0437	−0.0816	−0.0437	0.1689	0.1689
	3	241.696	244.838	247.980	0.0094	0.0287	0.0094	0.0475	0.0446
				Total $\sum\|\Delta V_i\|$				0.2329	0.2230
Tangential	1	1.5708	4.7124	7.8540	0.0021	−0.0042	0.0021	0.0082	0.0082
	2	121.131	124.272	127.414	−0.0170	−0.0014	0.0184	0.0368	0.0368
	3	240.235	243.376	246.518	−0.0117	0.0027	0.0081	0.0226	0.0145
				Total $\sum\|\Delta V_i\|$				0.0676	0.0595

Second, the relative longitude error $\Delta\delta\lambda_{\text{err}}$ can be also obtained by Eq. (36) such that

$$a\Delta\delta\lambda_{\text{err}} = a(\Delta\delta\lambda_{\text{real}} - \Delta\delta\lambda) = -2(\alpha_1\Delta V_{R_1} + \alpha_2\Delta V_{R_2} + \alpha_3\Delta V_{R_3})/n \quad (52)$$

where $\Delta\delta\lambda_{\text{real}}$ and $\Delta\delta\lambda$ are the real (with the thrust error) and the ideal relative longitude changes. The worst-case relative longitude error $|\delta\lambda^*_{\text{err}}|$ can be easily obtained by

$$na|\delta\lambda^*_{\text{err}}| = 2\sigma_\alpha|\Delta V_{R_1} + \Delta V_{R_2} + \Delta V_{R_3}| \quad (53)$$

with

$$\begin{pmatrix}\alpha_1^*\\ \alpha_2^*\\ \alpha_3^*\end{pmatrix} = \begin{pmatrix}\pm\sigma_\alpha\\ \pm\sigma_\alpha\\ \mp\sigma_\alpha\end{pmatrix} \quad (54)$$

when α_3^* has the opposite sign from (α_1^*, α_2^*), assuming the $(++-)$ combination in Table 2. The general solution of $(\alpha_1^*, \alpha_2^*, \alpha_3^*)$ can be obtained by

$$\begin{pmatrix}\alpha_1^*\\ \alpha_2^*\\ \alpha_3^*\end{pmatrix} = \begin{pmatrix}\pm(-1)^{k_1}\\ \pm(-1)^{k_2}\\ \pm(-1)^{k_3}\end{pmatrix}\sigma_\alpha \quad (55)$$

and the worst-case relative longitude error becomes

$$|\delta\lambda^*_{\text{err}}| = 2\sigma_\alpha\|\Delta\delta\boldsymbol{e}\| \quad (56)$$

Case b: $\Delta\delta\lambda^2 \geq 4\|\Delta\delta\boldsymbol{e}\|^2$

The case with larger along-track distance correction compared to relative eccentricity correction (i.e., $\Delta\delta\lambda^2 \geq 4\|\Delta\delta\boldsymbol{e}\|^2$) is considered. Final results are only presented since the derivation procedure is identical to the previous case: $\Delta\delta\lambda^2 < 4\|\Delta\delta\boldsymbol{e}\|^2$. Assuming $\Delta\delta\lambda \geq 0$ without loss of generosity, $|A|^*$ and $\|\delta\boldsymbol{e}^*_{\text{err}}\|$ can be derived by

$$|A|^* = |\alpha_1\Delta V_{R_1} + \alpha_2\Delta V_{R_2} - \alpha_3\Delta V_{R_3}|^* = \sigma_\alpha|\Delta V_{R_1} + \Delta V_{R_2} - \Delta V_{R_3}| = \sigma_\alpha na\Delta\delta\lambda/2 \quad (57)$$

$$\|\delta\boldsymbol{e}^*_{\text{err}}\| = |A|^*/na = \sigma_\alpha|\Delta\delta\lambda|/2 \quad (58)$$

when $(\alpha_1^*, \alpha_2^*, \alpha_3^*)$ satisfy Eq. (55). The worst-case relative longitude error $|\delta\lambda^*_{\text{err}}|$ becomes

$$|\delta\lambda^*_{\text{err}}| = \sigma_\alpha|\Delta\delta\lambda| \quad (59)$$

when $(\alpha_1^*, \alpha_2^*, \alpha_3^*)$ correspond to Eq. (50).

B. In-Plane Reconfiguration with Three Tangential Maneuvers

For comparison of robustness, the sensitivity study of the three tangential maneuver solution is also performed. Since $\Delta\delta a$ is assumed to be zero in this paper, only the $|\Delta\delta a| < \|\Delta\delta\boldsymbol{e}\|$ case in Ref. [10] is considered. It is assumed that the tangential maneuver method achieved the absolute minimum solution (i.e., $\sum|\Delta V_{T_i}| = na\|\Delta\delta\boldsymbol{e}\|/2$). Before going further, one of the ΔV_{T_i} combinations is selected as in Table 18, which will be generalized later.

First, the relative eccentricity vector control error is analyzed. While the ideal relative eccentricity correction is

$$\begin{aligned}a\Delta\delta e_x &= 2\Delta V_{T_1}\cos u_1/n + 2\Delta V_{T_2}\cos u_2/n + 2\Delta V_{T_3}\cos u_3/n\\ a\Delta\delta e_y &= 2\Delta V_{T_1}\sin u_1/n + 2\Delta V_{T_2}\sin u_2/n + 2\Delta V_{T_3}\sin u_3/n\end{aligned} \quad (60)$$

the relative eccentricity vector control error $(\delta e_{x,\text{err}}, \delta e_{y,\text{err}})$ due to the thrust error becomes

Table 18 Assumptions for in-plane reconfiguration sensitivity analysis

$\text{sign}(\cos u_1)$	$\text{sign}(\cos u_2)$	$\text{sign}(\cos u_3)$
$-$	$+$	$-$
$\text{sign}(\sin u_1)$	$\text{sign}(\sin u_2)$	$\text{sign}(\sin u_3)$
$+$	$-$	$+$
$\text{sign}(\Delta V_{T_1})$	$\text{sign}(\Delta V_{T_2})$	$\text{sign}(\Delta V_{T_3})$
$+$	$-$	$+$

$$\begin{aligned}an\delta e_{x,\text{err}} &= v\delta e_{x,\text{err}} = 2(\alpha_1\Delta V_{T_1} - \alpha_2\Delta V_{T_2} + \alpha_3\Delta V_{T_3})\cos u_1\\ an\delta e_{y,\text{err}} &= v\delta e_{y,\text{err}} = 2(\alpha_1\Delta V_{T_1} - \alpha_2\Delta v_{T_2} + \alpha_3\Delta V_{T_3})\sin u_1\end{aligned} \quad (61)$$

with the relative eccentricity vector 2-norm error:

$$n^2a^2\|\delta\boldsymbol{e}_{\text{err}}\|^2 = 4A^2 \quad (62)$$

The parameter A is redefined by

$$A \equiv \alpha_1\Delta V_{T_1} - \alpha_2\Delta V_{T_2} + \alpha_3\Delta V_{T_3} \quad (63)$$

Then, the worst-case relative eccentricity error becomes

$$\|\delta\boldsymbol{e}^*_{\text{err}}\| = 2|A|^*/na = \sigma_\alpha\|\Delta\delta\boldsymbol{e}\| \quad (64)$$

and the general (independent from the delta-v sign combinations) solution of $|A|^*$ can be achieved by

$$|A|^* = \sigma_\alpha(|\Delta V_{T_1}| + |\Delta V_{T_2}| + |\Delta V_{T_3}|) \quad (65)$$

The corresponding $(\alpha_1^*, \alpha_2^*, \alpha_3^*)$ are the same as Eq. (50).

Second, the relative SMA control error δa_{err} is derived. From Eq. (2),

$$a\Delta\delta a_{\text{err}} = 2(\alpha_1\Delta V_{T_1} + \alpha_2\Delta V_{T_2} + \alpha_3\Delta V_{T_3})/n \quad (66)$$

can be achieved, and the worst-case error becomes

$$|\delta a^*_{\text{err}}| = \sigma_\alpha\|\Delta\delta\boldsymbol{e}\| \quad (67)$$

The corresponding $(\alpha_1^*, \alpha_2^*, \alpha_3^*)$ combination is equivalent to Eq. (55).

Third, the relative longitude error is derived. The desired relative longitude at the final time of $u = u_F$ can be expressed in terms of $(\Delta V_{T_1}, \Delta V_{T_2}, \Delta V_{T_3})$ and (u_1, u_2, u_3) such that

$$na\delta\lambda(u_F) = -3(u_F - u_3)\Delta V_{T_3} - 3(u_F - u_2)\Delta V_{T_2} - 3(u_F - u_1)\Delta V_{T_1} \quad (68)$$

The relative longitude error then becomes

$$na\delta\lambda_{\text{err}} = -3A \quad (69)$$

where the parameter A is redefined by

$$A \equiv (u_F - u_3)\alpha_3\Delta V_{T_3} + (u_F - u_2)\alpha_2\Delta V_{T_2} + (u_F - u_1)\alpha_1\Delta V_{T_1} \quad (70)$$

The worst-case relative longitude error can be obtained by

$$|\delta\lambda^*_{\text{err}}| = 3|A|^*/na \quad (71)$$

where

Table 19 Maximum ROE errors induced by radial and tangential maneuvers

Maximum error (worst case)		$\|\delta\boldsymbol{e}^*_{\text{err}}\|$	$\|\delta a^*_{\text{err}}\|$	$\|\delta\lambda^*_{\text{err}}\|$
With three ΔV_R	$\Delta\delta\lambda^2 < 4\|\Delta\delta\boldsymbol{e}\|^2$	$\sigma_\alpha\|\Delta\delta\boldsymbol{e}\|$ when $\begin{pmatrix}\alpha_1^*\\ \alpha_2^*\\ \alpha_3^*\end{pmatrix} = \begin{pmatrix}\pm\sigma_\alpha\\ \pm\sigma_\alpha\\ \pm\sigma_\alpha\end{pmatrix}$	— —	$2\sigma_\alpha\|\Delta\delta\boldsymbol{e}\|$ when $\begin{pmatrix}\alpha_1^*\\ \alpha_2^*\\ \alpha_3^*\end{pmatrix} = \begin{pmatrix}\pm(-1)^{k_1}\\ \pm(-1)^{k_2}\\ \pm(-1)^{k_3}\end{pmatrix}\sigma_\alpha$
	$\Delta\delta\lambda^2 \geq 4\|\Delta\delta\boldsymbol{e}\|^2$	$\frac{\sigma_\alpha\Delta\delta\lambda}{2}$ when $\begin{pmatrix}\alpha_1^*\\ \alpha_2^*\\ \alpha_3^*\end{pmatrix} = \begin{pmatrix}\pm(-1)^{k_1}\\ \pm(-1)^{k_2}\\ \pm(-1)^{k_3}\end{pmatrix}\sigma_\alpha$	— —	$\sigma_\alpha\Delta\lambda$ when $\begin{pmatrix}\alpha_1^*\\ \alpha_2^*\\ \alpha_3^*\end{pmatrix} = \begin{pmatrix}\pm\sigma_\alpha\\ \pm\sigma_\alpha\\ \pm\sigma_\alpha\end{pmatrix}$
With three ΔV_T		$\sigma_\alpha\|\Delta\delta\boldsymbol{e}\|$ when $\begin{pmatrix}\alpha_1^*\\ \alpha_2^*\\ \alpha_3^*\end{pmatrix} = \begin{pmatrix}\pm\sigma_\alpha\\ \pm\sigma_\alpha\\ \pm\sigma_\alpha\end{pmatrix}$	$\sigma_\alpha\|\Delta\delta\boldsymbol{e}\|$ when $\begin{pmatrix}\alpha_1^*\\ \alpha_2^*\\ \alpha_3^*\end{pmatrix} = \begin{pmatrix}\pm(-1)^{k_1}\\ \pm(-1)^{k_2}\\ \pm(-1)^{k_3}\end{pmatrix}\sigma_\alpha$	$\frac{3\sigma_\alpha}{na}\sum(u_F-u_i)\|\Delta V_{T_i}\|$ when $\begin{pmatrix}\alpha_1^*\\ \alpha_2^*\\ \alpha_3^*\end{pmatrix} = \begin{pmatrix}\pm(-1)^{k_1}\\ \pm(-1)^{k_2}\\ \pm(-1)^{k_3}\end{pmatrix}\sigma_\alpha$

$$A^* = \sigma_\alpha((u_F-u_3)\alpha_3|\Delta V_{T_3}| + (u_F-u_2)\alpha_2|\Delta V_{T_2}| + (u_F-u_1)\alpha_1|\Delta V_{T_1}|) \tag{72}$$

The corresponding $(\alpha_1^*, \alpha_2^*, \alpha_3^*)$ combination is equivalent to Eq. (55). Further analysis of $|\delta\lambda^*_{\text{err}}|$ can be performed from the fact that $(u_F - u_1)$ and $(u_F - u_2)$ are always greater than 1 rad. Assuming $(u_F - u_3) > 1$ as well,

$$|\delta\lambda^*_{\text{err}}| = \frac{3\sigma_\alpha}{na}((u_F-u_3)|\Delta V_{T_3}| + (u_F-u_2)|\Delta V_{T_2}| + (u_F-u_1)|\Delta V_{T_1}|) \geq \frac{3k\sigma_\alpha}{na}(|\Delta V_{T_3}| + |\Delta V_{T_2}| + |\Delta V_{T_1}|) \tag{73}$$

with $k > 1$. Since $\sum|\Delta V_{T_i}| = na\|\Delta\delta\boldsymbol{e}\|/2$ is assumed (i.e., absolute optimal solution), Eq. (73) can be organized by

$$|\delta\lambda^*_{\text{err}}| \geq \frac{3k\sigma_\alpha}{2}\|\Delta\delta\boldsymbol{e}\| \tag{74}$$

Comparing to the relative longitude error in the radial maneuver approach in Eq. (55), the following inequality holds:

$$|\delta\lambda^*_{\text{err}}|_{\Delta V_R} = 2\sigma_\alpha\|\Delta\delta\boldsymbol{e}\| < \frac{3k\sigma_\alpha}{2}\|\Delta\delta\boldsymbol{e}\| \leq |\delta\lambda^*_{\text{err}}|_{\Delta V_T} \tag{75}$$

which states that $|\delta\lambda^*_{\text{err}}|$ from the tangential method is larger than that from the radial method when $(u_F - u_3) = k > 1.33$.

A set of the worst-case ROE control errors is summarized in Table 19.

The performed sensitivity analysis is verified by the numerical examples, which are also applied in Sec. V. The 3-sigma of the delta-v scale factor error σ_α is set to 0.05, and the worst-case analysis is conducted by assuming $(\alpha_1, \alpha_2, \alpha_3)$ as extreme values corresponding to the 3-sigma value. The two combinations of the $(\alpha_1, \alpha_2, \alpha_3)$ set are considered in Table 20. The results verify that the thrust error in the radial maneuvers merely affects the relative SMA error so that the relative longitude error is smaller than that with the tangential maneuvers. In addition, the resultant relative eccentricity errors are exactly the same in the two methods.

C. Control Accuracy

The ROE changes caused by a single burn of radial and tangential delta-v maneuvers are summarized in Table 21. The results aim to predict the required minimum thrust for the given ROE control accuracy requirements, especially on the in-plane ROE: $\delta\boldsymbol{e}$, δa, and $\delta\lambda$. As shown in the table, $\delta\boldsymbol{e}$ can be controlled with ΔV_R two times as accurate as with ΔV_T due to the nature of dynamics in Eq. (2). Despite the large fuel consumption, the radial impulsive maneuver strategy could be an option if higher control accuracy is desirable for the given mission requirements. In addition, although the radial impulse induces $\delta\lambda$ instantaneously, unlike the tangential impulse,

Table 20 Sensitivity analysis for reconfiguration scenarios 1 to 3

			$a\|\delta\boldsymbol{e}^*_{\text{err}}\|$, m	$a\|\delta a^*_{\text{err}}\|$, m	$a\|\delta\lambda^*_{\text{err}}\|$, m
Scenario 1	With three ΔV_R	Combination 1 $\begin{pmatrix}\alpha_1^*\\ \alpha_2^*\\ \alpha_3^*\end{pmatrix} = \begin{pmatrix}\pm\sigma_\alpha\\ \pm\sigma_\alpha\\ \pm\sigma_\alpha\end{pmatrix}$	0.7500	— —	0
		Combination 2 $\begin{pmatrix}\alpha_1^*\\ \alpha_2^*\\ \alpha_3^*\end{pmatrix} = \begin{pmatrix}\pm(-1)^{k_1}\\ \pm(-1)^{k_2}\\ \pm(-1)^{k_3}\end{pmatrix}\sigma_\alpha$	0	— —	1.5000
	With three ΔV_T	Case 1	0.7500	0	0
		Case 2	0	0.7500	8.8357
Scenario 2	With three ΔV_R	Case 1	0.7500	— —	15.0000
		Case 2	7.5000	— —	1.5000
	With three ΔV_T	Case 1	0.7500	0	15.0000
		Case 2	0	0.7500	6.1643
Scenario 3	With three ΔV_R	Case 1	0.7500	— —	1.0000
		Case 2	0.5000	— —	1.5000
	With three ΔV_T	Case 1	0.7500	0	1.0000
		Case 2	0	0.7500	7.8357

Table 21 In-plane ROE control accuracy from single minimum impulse

Control precision	$\delta \boldsymbol{e}$	δa	$\delta\lambda$
With ΔV_R	$\frac{1}{na}\Delta V_{\min}$	— —	$\frac{2}{na}\Delta V_{\min}$
With ΔV_T	$\frac{2}{na}\Delta V_{\min}$	$\frac{2}{na}\Delta V_{\min}$	— —

it can avoid changing δa; otherwise, it not only shifts δa but also drifts $\delta\lambda$ over time.

VII. Conclusions

A radial maneuver strategy with two- and three-impulsive burns for formation reconfiguration was proposed. While the total delta-v costs of the two and three impulses are the same, the three-impulse method has the advantage of distributing the impulses more evenly among the impulses while the total delta-v costs are the same between the two- and three-impulse methods. Despite a clear limitation of employing only radial maneuvers in fuel efficiency compared to the tangential maneuver strategy, two advantages were addressed supported by the numerical results. The first is that its total delta-v magnitude is independent of the allowed reconfiguration time assuming that it is longer than 1.5 orbit periods, and the second is that the ROE control errors become less sensitive to the thrust model errors. Considering that most CubeSats are incapable of performing formation keeping in a regular basis, it is important to keep the along-track distance for safety. In this regard, the SMA control error caused by the tangential maneuver error can be critical since it can make the spacecraft approaching to each other. The proposed radial maneuver strategy, on the other hand, hardly induces the SMA control error even with the thrust errors so that the intersatellite distance can be maintained robustly.

A possible long-term reconfiguration strategy employing the proposed radial maneuver strategy can be described as follows. The SMA is controlled by differential drag, as well as the relative longitude, to the maximum extent under given reconfiguration time; and then the radial impulses correct the residual relative longitude together with the relative eccentricity. This long-term strategy will benefit from the increased robustness against the thrust errors in tradeoff of delta-v increase. For future work, a tradeoff study between a delta-v cost and safety will be carried out, for long-term operations of CubeSats.

Acknowledgment

The research of the first author is partly supported by Deutsches Zentrum für Luft- und Raumfahrt (DLR, German Space Center) under grant no. 50 RU 1803.

References

[1] Ichimura, Y., and Ichikawa, A., "Optimal Impulsive Relative Orbit Transfer Along a Circular Orbit," *Journal of Guidance, Control, and Dynamics*, Vol. 31, No. 4, 2008, pp. 1014–1027. https://doi.org/10.2514/1.32820

[2] Wiesel, W. E., "Optimal Impulsive Control of Relative Satellite Motion," *Journal of Guidance, Control, and Dynamics*, Vol. 26, No. 1, 2003, pp. 74–78. https://doi.org/10.2514/2.5016

[3] Lovell, T. A., and Tragesser, S. G., "Guidance for Relative Motion of Low Earth Orbit Spacecraft Based on Relative Orbit Elements," *AIAA/AAS Astrodynamics Specialist Conference and Exhibit*, AIAA Paper 2004-4988, 2014. https://doi.org/10.2514/6.2004-4988

[4] Schaub, H., "Relative Orbit Geometry Through Classical Orbit Element Differences," *Journal of Guidance, Control, and Dynamics*, Vol. 27, No. 5, 2004, pp. 839–848. https://doi.org/10.2514/1.12595

[5] Vadali, S. R., Schaub, H., and Alfriend, K. T., "Initial Conditions and Fuel Optimal Control for Formation Flying of Satellites," *AIAA Guidance, Navigation, and Control Conference*, AIAA Paper 1999-4265, 1999. https://doi.org/10.2514/6.1999-4265

[6] Schaub, H., and Alfriend, K. T., "Impulsive Feedback Control to Establish Specific Mean Orbit Elements of Spacecraft Formations," *Journal of Guidance, Control, and Dynamics*, Vol. 24, No. 4, 2001, pp. 739–745. https://doi.org/10.2514/2.4774

[7] Vaddi, S. S., Alfriend, K. T., Vadali, S. R., and Sengupta, P., "Formation Establishment and Reconfiguration Using Impulsive Control," *Journal of Guidance, Control, and Dynamics*, Vol. 28, No. 2, 2005, pp. 262–268. https://doi.org/10.2514/1.6687

[8] D'Amico, S., and Montenbruck, O., "Proximity Operations of Formation-Flying Spacecraft Using an Eccentricity/Inclination Vector Separation," *Journal of Guidance, Control, and Dynamics*, Vol. 29, No. 3, 2006, pp. 554–563. https://doi.org/10.2514/1.15114

[9] D'Amico, S., "Autonomous Formation Flying in Low Earth Orbit," Ph.D. Thesis, Delft Univ. of Technology, Delft, The Netherlands, 2010.

[10] Gaias, G., and D'Amico, S., "Impulsive Maneuvers for Formation Reconfiguration Using Relative Orbital Elements," *Journal of Guidance, Control, and Dynamics*, Vol. 38, No. 6, 2015, pp. 1036–1049. https://doi.org/10.2514/1.G000189

[11] Gaias, G., and Ardaens, J.-S., "Flight Demonstration of Autonomous Noncooperative Rendezvous in Low Earth Orbit," *Journal of Guidance, Control, and Dynamics*, Vol. 41, No. 6, 2018, pp. 1337–1354. https://doi.org/10.2514/1.G003239

[12] Mok, S. H., Choi, Y., Bang, H., and Leeghim, H., "A Delayed Impulse Control Strategy for Spacecraft Formations," *Journal of the Astronautical Sciences*, Vol. 60, Nos. 3–4, 2013, pp. 337–365. https://doi.org/10.1007/s40295-015-0055-z

[13] Prussing, J. E., "A Class of Optimal Two-Impulse Rendezvous Using Multiple-Revolution Lambert Solutions," *Journal of the Astronautical Sciences*, Vol. 48, Nos. 2–3, 2000, pp. 131–148.

[14] Shen, H., and Tsiotras, P., "Optimal Two-Impulse Rendezvous Using Multiple-Revolution Lambert Solutions," *Journal of Guidance, Control, and Dynamics*, Vol. 26, No. 1, 2003, pp. 50–61. https://doi.org/10.2514/2.5014

[15] Zhang, G., Zhou, D., and Mortari, D., "Optimal Two-Impulse Rendezvous Using Constrained Multiple-Revolution Lambert Solutions," *Celestial Mechanics and Dynamical Astronomy*, Vol. 110, No. 4, 2011, pp. 305–317. https://doi.org/10.1007/s10569-011-9349-z

[16] Koenig, A. W., and D'Amico, S., "Robust and Safe N-Spacecraft Swarming in Perturbed Near-Circular Orbits," *Journal of Guidance, Control, and Dynamics*, Vol. 41, No. 8, 2018, pp. 1643–1662. https://doi.org/10.2514/1.G003249

[17] Foster, C., Hallam, H., and Mason, J., "Orbit Determination and Differential-Drag Control of Planet Labs Cubesat Constellations," *AAS/AIAA Astrodynamics Specialist Conference*, American Astronautical Society, AAS Paper 15-524, Springfield, VA, Aug. 2015.

[18] Foster, C., Mason, J., Vittaldev, V., Leung, L., Beukelaers, V., Stepan, L., and Zimmerman, R., "Differential Drag Control Scheme for Large Constellation of Planet Satellites and On-Orbit Results," *International Workshop on Satellite Constellations and Formation Flying*, International Astronautical Federation, IWSCFF Paper 17-33, Paris, France, June 2017.

[19] Bussy-Virat, C. D., Ridley, A. J., Masher, A., Nave, K., and Intelisano, M., "Assessment of the Differential Drag Maneuver Operations on the CYGNSS Constellation," *IEEE Journal of Selected Topics in Applied Earth Observations and Remote Sensing*, Vol. 12, No. 1, 2019, pp. 7–15. https://doi.org/10.1109/JSTARS.2018.2878158

[20] Koenig, A. W., Guffanti, T., and D'Amico, S., "New State Transition Matrices for Spacecraft Relative Motion in Perturbed Orbits," *Journal of Guidance, Control, and Dynamics*, Vol. 40, No. 7, 2017, pp. 1749–1768. https://doi.org/10.2514/1.G002409

[21] Schaub, H., and Junkins, J. L., *Analytical Mechanics of Space Systems*, Appendix F, AIAA Education Series, AIAA, Reston, VA, 2018. https://doi.org/10.2514/4.105210

[22] Gaias, G., D'Amico, S., and Andaens, J. S., "Generalised Multi-Impulsive Manoeuvres for Optimum Spacecraft Rendezvous in Near-Circular Orbit," *International Journal of Space Science and Engineering*, Vol. 3, No. 1, 2015, pp. 68–88. https://doi.org/10.1504/IJSPACESE.2015.069361